Numerical Heat Transfer Part B: Fundamentals, Volume 48, Number 3, September 2005, pp. 235-256

A Study of LES Stress and Flux Models Applied to a Buoyant Jet.

Jude Worthy & Philip Rubini

Jude Worthy, Department of Aerospace Sciences, Cranfield University, UK, MK43 0AL.

Currently at Department of Mathematics, University of North Carolina at Chapel Hill, USA, 27599-3250.

Philip Rubini, Department of Aerospace Sciences, Cranfield University, MK43 0AL.

Mailing address:

Jude Worthy

Department of Mathematics

Philips Hall

PH320

University of North Carolina at Chapel Hill

Chapel Hill, NC, 27599

Running Head: LES of Buoyant Jet

Abstract

LES stress and scalar flux subgrid scale models are evaluated in the context of buoyant jets. Eddy viscosity, eddy diffusivity (including formulations of the generalized gradient diffusion hypothesis), 'structure' (Bardina and Leonard), mixed and dynamic models are scrutinized. The performance of the models is examined in terms of the main flow variables and also with respect to the 'internal' behavior of the models in terms of the relative contributions to the turbulent kinetic energy budget.

Nomenclature

B buoyancy term

DF diffusion term

DP dissipation term

ENJ J flux component

$Fr = U^2 / gL$ Froude number

k turbulent/ subgrid kinetic energy.

P turbulent energy production term

$\mathrm{Pr} = \upsilon / \alpha$ Prandtl number

q_j subgrid flux

$\mathrm{Re} = UL / \upsilon$ Reynolds number

T temperature

TIJ IJ stress component

u/v/w velocities

UU/VV/WW turbulent kinetic energy components

α thermal conductivity

β coefficient of thermal expansion

δ_{ij} Kronecker delta

Δ filter width, grid width

ε temperature difference, dissipation term

κ frequency

μ viscosity

Π reduced pressure term

ρ density

τ_{ij} stress tensor

υ kinematic viscosity

Subscripts

$X_i / X_j / X_k$ components to be considered over three dimensions

X_a ambient value

X_0 initial / input value

X_t turbulent value – turbulent Prandtl number or turbulent viscosity

X_b Boussinesq term

X_{sgs} subgrid scale term

Superscripts

$\overline{X}$ filtered variable with arbitrary filter

$\tilde{\tilde{X}}$ filtered variable with arbitrary filter

$\overrightarrow{X}$ filtered variable with arbitrary filter

$\widetilde{X}$ Favre-filtered variable with arbitrary filter

X' fluctuating component of filtered variable

Abbreviations and Acronyms

CFD	Computational Fluid Dynamics
DNS	Direct numerical simulation
GGDH	Generalised gradient diffusion hypothesis
LDM	Localised Dynamic Model
LES	Large eddy simulation
LMN	Low Mach number
RANS	Reynolds-averaged Navier-Stokes
SGDH	Standard gradient diffusion hypothesis
SKE	Subgrid kinetic energy
TKE	Turbulent kinetic energy

1. Introduction

Large Eddy Simulation (LES) was first introduced by Lilly [1] and Smagorinsky [2]. The concept provides a formalism which enables time accurate simulations of turbulent flows to be carried out for a filtered velocity field, as opposed to a time averaged velocity field in the corresponding Reynolds Averaged (RANS) approach, at less computational cost than a corresponding direct numerical simulation (DNS) in which all the scales of motion are fully resolved. The initial growth and acceptance of LES as a viable computational approach was initially constrained by available computing resources. However as computing power has steadily increased and become more readily available, interest in the technique has grown, perhaps most significantly with the development of the dynamic procedure of Germano [3].

Whilst the concept of LES, and the use of a sub-grid scale turbulence model, has not changed, alternative sub-grid scale models continue to be proposed. In this state of ongoing development it is difficult to ensure that representative benchmark comparisons of models are carried out. There

are only a limited number of publications which provide a comparative assessment of models, the works of Bastiaans et al. [4, 5] are particularly notable, and this present paper has a similar objective. Other buoyant jet LES simulations have been performed [6, 7], which focus on the simulation of the buoyant jet particularly rather than the LES model as done here. No hypothesis was followed, so the work may be considered to be a series of 'numerical experiments', as Lilly [1] described them, with conclusions and observations drawn from the results of the simulations.

The physical problem of a buoyant jet was selected as the basis to assess the models. Buoyant jets incorporate laminar flow, transition, and fully turbulent flow, and are representative of a wide range of practical applications including building heating and ventilation, fire safety and the dispersion of pollutants in the atmosphere.

The principle objective of this work was to assess the relative behavior of the LES sub-grid scale stress and scalar flux models and to provide a recommendation for which model to adopt for buoyant jet simulations.

2. Filtered Governing Equations

LES, similarly to RANS, is based upon a filtering of the governing equations to reduce the scales which are to be resolved. RANS may be considered as filtering out temporal variation, whereas LES filters out the spatial subgrid scales, i.e. those scales of motion which cannot be represented due to the coarseness of the grid. Germano [3] gives a full introduction to filtering and the relation between filter scales.

From the instantaneous variable and the instantaneous filtered variable at a point in space we define the 'fluctuating' component, in a manner analogous to the RANS approach, although the fluctuations are in space: $f' = f - \bar{f}$. The filtered governing equations are obtained by applying the filter to each term in the governing equations of motion appropriate to the flow under

consideration. In this work these were the Low Mach Number equations as derived by Paulucci [8], and Rehm and Baum [9]. This form of the Navier-Stokes equations my be considered to lie between the full compressible Navier-Stokes equations and the (Boussinesq) incompressible Navier-Stokes equations. It is assumed that sound waves are propagated at infinite speed, allowing the pressure term to be solved with a fast elliptic solver, but the density and temperature variations are not limited to the Boussinesq approximation. In order to accommodate fluctuations of density, the Favre-average, $\widetilde{f} = \overline{\rho f} / \overline{\rho}$, is employed in conjunction with the filter.

The resultant form of the governing equations, comprising the continuity, the momentum, the temperature equation, and the equation of state are given below.

$$\frac{\partial \overline{\rho}}{\partial t} + \frac{\partial \overline{\rho} \widetilde{u}_i}{\partial x_i} = 0 \tag{2.1}$$

$$\frac{\partial \overline{\rho} \widetilde{u}_i}{\partial t} + \frac{\partial \overline{\rho} \widetilde{u}_i \widetilde{u}_j}{\partial x_j} = -\frac{\partial \overline{\Pi}}{\partial x_i} + \frac{1}{\mathrm{Re}} \frac{\partial^2 \widetilde{u}_i}{\partial x_j^{\,2}} + \frac{1}{Fr} (\overline{\rho} - 1) g_i - \frac{\partial \overline{\rho} \tau_{ij}}{\partial x_j} \tag{2.2}$$

$$\frac{\partial \widetilde{T}}{\partial t} + \widetilde{u}_j \frac{\partial \widetilde{T}}{\partial x_j} = \frac{1}{\overline{\rho}} \frac{1}{\mathrm{Re}\,\mathrm{Pr}} \frac{\partial^2 \widetilde{T}}{\partial x_j^{\,2}} - \frac{\partial q_j}{\partial x_j} \tag{2.3}$$

$$\overline{\rho} \widetilde{T} = 1 \tag{2.4}$$

The momentum subgrid terms, $\tau_{ij} = \overline{\overline{u_i u_j}} - \widetilde{u}_i \widetilde{u}_j$, are called the stresses, and the temperature subgrid terms, $q_j = \overline{\overline{u_j T}} - \widetilde{u}_j \widetilde{T}$ are called the fluxes, and these must be modelled. The double bar as well as the tilda represents the Favre average.

The assumption was made that the density varies slowly through space and that therefore the approximation $\bar{f} = \widetilde{f}$ was valid. The viscous term in the momentum equation and the state equation are then achievable in this form.

The subgrid decomposition [10] of the stress tensor into more elementary parts becomes,

$$\tau_{ij} = \overline{u_i u_j} - \overline{u}_i \overline{u}_j \qquad (2.5)$$

$$= \overline{\overline{u}_i \overline{u}_j} - \overline{u}_i \overline{u}_j \qquad \text{Leonard term}$$

$$+ \overline{u_i' \overline{u}_j} + \overline{\overline{u}_i u_j'} \qquad \text{Cross term}$$

$$+ \overline{u_i' u_j'} \qquad \text{Reynolds term}$$

The Leonard terms represent the largest of the subgrid scales, followed by the Cross terms and finally the Reynolds terms.

3. LES Models

The first LES models [1,2] were purely diffusive in nature, which is a sufficient quality to enable a solution with an explicit numerical scheme. Piomelli [11] highlights the main objectives and challenges of LES modelling. The first is this diffusive quality, which can largely be associated with the Reynolds term. The second is to accurately capture the backscatter of the energy – that is that the turbulent kinetic energy travels from small scales to large scales as well as from large to small. Thirdly for the model to be internally accurate; that is that the terms in the subgrid decomposition are individually accurately represented. The final consideration is the computational cost to implement the models. Schumann [12] introduced full second moment modelling (providing a transport equation for each of the stresses and fluxes) but this was not pursued due to cost and the further modelling requirements.

Boussinesq Hypothesis. The Boussinesq hypothesis is *that the turbulent terms can be modelled as directly analogous to the molecular viscosity terms using a 'turbulent viscosity'*. This can be written (not necessarily equivalently) in a number of forms, the simplest of which is used here.

$$\tau_{ij} = -2\upsilon_t \overline{S}_{ij} \tag{3.1}$$

This is usually called the eddy viscosity model, and encompasses a variety of different models determined by the evaluation of the turbulent viscosity, υ_t. The standard gradient diffusion hypothesis (SGDH), also the eddy diffusivity model, is given by

$$q_j = \frac{\upsilon_t}{\mathrm{Pr}_t}\frac{\partial T}{\partial x_j} \tag{3.2}$$

Dimensional reasoning shows $\upsilon_t = C\widetilde{\varepsilon}^{1/3}\Delta^{4/3}$, where $\widetilde{\varepsilon}$ is the energy transfer through the cutoff in the energy spectrum (see Sagaut [13]), and Δ is the filter width.

The turbulent Prandtl number is typically chosen to be a constant although dynamic procedures can also be applied to it. This has received considerably less attention, and improved models here are desirable.

Smagorinsky model The original LES model was the Smagorinsky model [2,1] where the turbulent viscosity is given by

$$\upsilon_t = C\Delta^2\left|\overline{S}\right| \ , \ \left|\overline{S}\right| = (2\overline{S}_{ij}\overline{S}_{ij})^{1/2} \tag{3.3}$$

Lilly [14] showed the model to be consistent with the Kolmogorov spectrum if the correct constant, 0.03, is chosen, although a constant of 0.01 is typically used after numerical experiments, for example [15].

Buoyancy-Modified Smagorinsky Model This was developed by Lilly [1]. Note the buoyancy term does reintroduce a non-dimensional flow parameter into the model. The original derivation makes an approximation only suitable for low Mach number flows. The model is given by

$$\upsilon_t = C\Delta^2(2\overline{S}_{ij}\overline{S}_{ij} - \frac{1}{Fr\,\mathrm{Pr}_t}\frac{\partial \overline{T}}{\partial x_i}\delta_{ij})^{1/2} \tag{3.4}$$

Structure Function model The structure function in physical space is an extension of the spectral eddy viscosity model, developed by Metais and Lesieur [16]. It takes the following form [17].

$$\upsilon_t = 0.063\Delta(F_2(x,\Delta))^{1/2} \tag{3.5}$$

in which $F_2(x,\Delta) =< \left\|\bar{u}(x,t) - \bar{u}(x+r,t)\right\|^2 >$ (3.6)

The structure function F_2 is calculated as the average of the values made with the six immediately adjacent cells. In Eq. (3.6), the double side bars are the magnitude of the vector, and the pointed brackets represent the average over all suitable vectors r with magnitude Δ.

One Equation Model The one equation model [12] uses a transport equation for the subgrid kinetic energy and uses the Boussinesq hypothesis also.

$$\upsilon_t = C\Delta(k_{sgs})^{1/2} \tag{3.7}$$

$C = 0.069$, and is a theoretically derived value [13]. However, values between 0.04 and 1 have been used [18]. The transport equation can be given by

$$\frac{\partial k}{\partial t} + \frac{\partial u_j k}{\partial x_j} = +\upsilon \frac{\partial^2 k}{\partial x_j \partial x_j} + P - DP + DF + B \tag{3.8}$$

in which $P = -\tau_{ij}\frac{\partial \bar{u}_i}{\partial x_j}$, $DP = C_1\frac{(k)^{3/2}}{\bar{\Delta}}$, $DF = C_2\frac{\partial}{\partial x_j}(\Delta(k)^{1/2}\frac{\partial k}{\partial x_j})$, and $B = (\overline{u_j\rho} - \bar{u}_j\bar{\rho})g_j$. P is the regular production term, DP is the dissipation term, DF is the diffusion term, and B is the production due to buoyancy.

The constants are found to take the values $C_1 = 1$ and $C_2 = 0.1$. The buoyancy term is given by the density flux and is modeled according to whichever method is preferred. It is usually modeled with the standard gradient diffusion hypothesis.

Generalised Gradient Diffusion Hypothesis The generalized gradient diffusion hypothesis (GGDH) has been found in RANS modeling [19, 20] to give significant improvements. Daly and

Harlow [21] were among the first to derive this model, although it was largely overlooked. The model is derived from balance considerations from the scalar flux equation (the equivalent of the TKE equation for the temperature fluctuations), assuming steady homogeneous turbulence, and assuming that higher order correlations are negligible, although the temperature (or scalar) flux is itself of the order of the neglected terms.

$$q_j = c_t \frac{k}{\varepsilon} \tau_{jk} \frac{\partial T}{\partial x_k} \tag{3.9}$$

This can be modeled with $\varepsilon = \frac{k^{3/2}}{\Delta}$, using k from the transport equation if used, or from $k = \frac{1}{2}\tau_{ii}$. Substitution results in the following.

$$q_j = -c_t \Delta k^{-0.5} \tau_{jk} \frac{\partial T}{\partial x_k} \tag{3.10}$$

$$\text{or } q_j = -c_t \Delta (\tfrac{1}{2}\tau_{ii})^{-0.5} \tau_{jk} \frac{\partial T}{\partial x_k} \tag{3.11}$$

Equation 3.17 is labeled GGDH_1, and Equation 3.18 is GGDH_2.

Bardina Model The Bardina model [22] was the first of the scale similarity models. The basic principle behind such models is that the structure of the smallest resolved scales, given by the filtered subgrid component, is similar to the structure of the largest unresolved scales, given by the subgrid component. This implies correctly that the Leonard term is dominant in the stress decomposition giving

$$\tau_{ij} = \overline{\overline{u}_i \overline{u}_j} - \overline{\overline{u}_i}\,\overline{\overline{u}_i} \tag{3.12}$$

Leonard Model Leonard [10] introduced the Taylor expansion models of which there are two main formulations. The form that Leonard gives takes the linear expansion of the components $\overline{u}_i$ and $\overline{u}_j$, whereas Kwak [23] takes the expansion around $\overline{u}_i \overline{u}_j$. We use Leonard's form for both the stress and the flux.

$$\overline{\overline{u}_i\overline{u}_j} = \overline{u}_i\overline{u}_j + \frac{\overline{\Delta}^2}{24}\frac{\partial\overline{u}_i}{\partial x_k}\frac{\partial\overline{u}_j}{\partial x_k} + O(\overline{\Delta}^2) \qquad \text{Leonard [10]} \qquad (3.13)$$

$$\overline{\overline{u}_i\overline{u}_j} = \overline{u}_i\overline{u}_j + \frac{\overline{\Delta}^2}{24}\frac{\partial^2\overline{u}_i\overline{u}_j}{\partial x_k{}^2} + O(\overline{\Delta}^3) \qquad \text{Kwak et al. [23]} \qquad (3.14)$$

$$\overline{\overline{u}_i\overline{T}} = \overline{u}_i\overline{T} + \frac{\overline{\Delta}^2}{24}\frac{\partial\overline{u}_i}{\partial x_k}\frac{\partial\overline{T}}{\partial x_k} + O(\overline{\Delta}^2) \qquad (3.15)$$

Mixed Models There are two natural types of mixed model., $\tau_{ij} = \frac{1}{2}(A+B)$, type 1, and $\tau_{ij} = L + C + R$, type 2. Bardina et al. [22] were the first to propose a mixed model. They proposed a type 1 model using the Smagorinsky combined with the Bardina. This is appropriate since both are models for the whole stress, and it combines the dissipation of the Smagorinsky with the structural accuracy of the Bardina.

$$\tau_{ij} = \tfrac{1}{2}(-2\upsilon_{sgs}\overline{S}_{ij} + \overline{\overline{u}_i\overline{u}_j} - \overline{\overline{u}_i}\,\overline{\overline{u}_j}) \qquad (3.16)$$

Type 2 models mix separate models of the different components of the Leonard decomposition. The Cross terms can be modeled as identical to the Leonard term. An example would be the one-equation model with the Leonard model, with or without explicitly modeling the Cross terms.

Dynamic models Dynamic models allow the empirical constants of the previous models to be evaluated locally in space and time, and overcome some problems of the static (non-dynamic) models. Germano et al. [24] introduced the first dynamic model, the dynamic Smagorinsky, based on an algebraic identity, which Germano [3] generalises for use with any other appropriate model. Considering double filtered terms the following holds.

$$\overleftrightarrow{u_iu_j} - \overleftrightarrow{\overline{u}_i\overline{u}_j} = \overleftrightarrow{u_iu_j} - \overleftrightarrow{\overline{u}_i\overline{u}_j} + \overleftrightarrow{\overline{u}_i\overline{u}_j} - \overleftrightarrow{\overline{u}_i}\,\overleftrightarrow{\overline{u}_j} \qquad (3.17)$$

This can be rewritten

$$T_{ij} = \overleftrightarrow{\tau_{ij}} + L_{ij} \qquad (3.18)$$

where $T_{ij} = \overleftrightarrow{u_iu_j} - \overleftrightarrow{\overline{u}_i}\,\overleftrightarrow{\overline{u}_j}$, $\tau_{ij} = \overline{u_iu_j} - \overline{u}_i\overline{u}_j$ and $L_{ij} = \overleftrightarrow{\overline{u}_i\overline{u}_j} - \overleftrightarrow{\overline{u}_i}\,\overleftrightarrow{\overline{u}_j}$.

This relates exactly the subgrid stress of the double filtered field to the filtered (with the second filter) subgrid stress of the single filtered field via a quantity calculable from the filtered variables.

Putting an arbitrary SGS model into the stress tensors, which takes a form such that $\tau_{ij} = Cf(\overline{u}_i)$, and $T_{ij} = Cf(\overleftrightarrow{u}_i)$ we find

$$Cf(\overleftrightarrow{u}_i) = \overleftrightarrow{Cf(\overline{u}_i)} + L_{ij} \tag{3.19}$$

We have two basic evaluation types.

$$Cf(\overleftrightarrow{u}_i) = C\overleftrightarrow{f(\overline{u}_i)} + L_{ij} \qquad \text{Type 1 evaluation.} \tag{3.20}$$

$$C^{n+1} f(\overleftrightarrow{u}_i) = \overleftrightarrow{C^n f(\overline{u}_i)} + L_{ij} \qquad \text{Type 2 evaluation.} \tag{3.21}$$

n in the type 2 evaluation is the time step. A problem is that the constant is typically taken out the filter term, to form the type 1 evaluation. Since it is only locally a constant, this is not strictly allowed. Lilly [14] proposes that if the flow has at least one homogeneous axis, the constant can be evaluated consistently by filtering only in the homogeneous axes. Piomelli and Liu [25] and Davidson [26] use the type 2 evaluation which is marginally more accurate than type 1.

Whichever evaluation is used the constant is over-prescribed with six equations describing it. Lilly [14] proposed a least squares approach to determine the final constant which has become the prevailing method.

Dynamic Smagorinsky Model Substituting the Smagorinsky model into the dynamic procedure previously described we have

$$L_{ij} = T_{ij} - \overleftrightarrow{\tau_{ij}} = \overleftrightarrow{\overline{u}_i \overline{u}_j} - \overleftrightarrow{\overline{u}}_i \overleftrightarrow{\overline{u}}_j \tag{3.22}$$

with $\overline{\tau_{ij}} = -2C\overline{\Delta}^2 \overleftrightarrow{|\overline{S}|\overline{S}_{ij}}$ and $T_{ij} = -2C\overleftrightarrow{\overline{\Delta}}^2 \left|\overleftrightarrow{\overline{S}}\right| \overleftrightarrow{\overline{S}}_{ij}$. Let $M_{ij} = (-2\overleftrightarrow{\overline{\Delta}}^2 \left|\overleftrightarrow{\overline{S}}\right| \overleftrightarrow{\overline{S}}_{ij} + 2\overline{\Delta}^2 \overleftrightarrow{|\overline{S}|\overline{S}_{ij}})$, then

$$C = \tfrac{1}{2}(L_{ij} M_{ij} / M_{kl} M_{kl}) \tag{3.23}$$

Lund et al. [27] investigate the numerical stability of negative viscosities, and find that the constant must be clipped, ensuring a non-negative value, in order to produce a stable result. The instability caused by near zero denominators in laminar flow can also be a problem. Balaras and Benocci [28], simulating a square duct flow, found that the constant has to be bounded above in some cases.

Dynamic Mixed Models The dynamic mixed model appeared soon after the Germano identity. Zang et al. [29] use the original mixed model of Bardina et al. [30], combining the Bardina model with the Smagorinsky model as the base model for the dynamic procedure.

$$\tilde{\tau}_{ij} = -2C\overline{\Delta}^2 \overleftrightarrow{\left|\overline{S}\right|\overline{S}_{ij}} + \overleftrightarrow{B_{ij}(\overline{u}_i, \overline{u}_j)} \tag{3.24}$$

$$T_{ij} = -2C\tilde{\overline{\Delta}}^2 \left|\tilde{\overline{S}}\right|\tilde{\overline{S}}_{ij} + B_{ij}(\tilde{\overline{u}}_i, \tilde{\overline{u}}_j) \tag{3.25}$$

where $B_{ij}(\overline{u}_i, \overline{u}_j) = \overleftarrow{\overline{u}_i \overline{u}_j} - \overleftarrow{\overline{u}}_i \overleftarrow{\overline{u}}_j$ (3.26)

or $B_{ij}(\overline{u}_i, \overline{u}_j) = \overline{\overline{u}_i \overline{u}_j} - \overline{\overline{u}}_i \overline{\overline{u}}_j$ (3.27)

Equation 3.25 gives the formulation with an unspecified second filter, and Vreman et al. [30] give the form in equation 3.27. The distinction is that in equation 3.26, the top filter (the single arrowhead is different from the double arrowhead filters) does not depend on the filters used 'below' whether a single filter, or a double filter as is the case for the test filter. The second formulation, equation 3.27, uses whichever filter or filters are used for the variable, so for the test filter this would incorporate a total of four filter layers.

Let $G_a = \overline{\Delta}^2 \overleftrightarrow{\left|\overline{S}\right|\overline{S}_{ij}}$, $G_b = \tilde{\overline{\Delta}}^2 \left|\tilde{\overline{S}}\right|\tilde{\overline{S}}_{ij}$, $H_a = \overleftrightarrow{B_{ij}(\overline{u}_i, \overline{u}_j)}$, and , then

$$C = (L_{ij} + H_a - H_b)/(G_a - G_b) \tag{3.28}$$

The constant still needs to be clipped, although backscatter can now occur through the addition of the Bardina model in a stable manner.

Localized Dynamic Model This model is the dynamic version of the one-equation model. A number of authors have developed it independently with different considerations [31, 32, 33, 34]. The first part applies the Germano identity to the subgrid model. Using the dynamic procedure with $\tau_{ij} = C\bar{\Delta}k^{1/2}\bar{S}_{ij}$, $T_{ij} = C\hat{\bar{\Delta}}K^{1/2}\overleftrightarrow{\bar{S}}_{ij}$, and using type 1 evaluation for C, let

$$M_{ij} = \overleftrightarrow{\bar{\Delta}}K^{1/2}\overleftrightarrow{\bar{S}}_{ij} - \overleftrightarrow{\bar{\Delta}k^{1/2}\bar{S}_{ij}} \tag{3.29}$$

Then $C = \dfrac{L_{ij}M_{ij}}{M_{kl}M_{kl}}$ (3.30)

K can be evaluated from a second transport equation, or from the relation $K = \overleftrightarrow{k} + L_{ii}$. The dynamic evaluation of the transport terms are given in appendix 1.

4. Simulation Details and Numerical Method

A buoyant jet similar to the experiment of Shabbir and George [34] and the simulation of Zhou et al. [15]. The simulations were obtained on a uniform grid of 63x127x63 cells over a solution domain of 7x14.11x7 (non-dimensionalised by the jet inlet diameter), with 9 cells across the jet inlet. Taking the ambient temperature to be 300K , this yields $\mathrm{Re} = 1300$, $Fr = 1.54$, and $\varepsilon = 0.893$, where the inflow temperature is given by $1 + \varepsilon$. $\mathrm{Pr} = 0.7$.

Open boundary conditions were employed at the sides and top of the computational domain, and special care had to be taken to ensure stability of the resulting simulations. Gresho [35] noted the critical issue of maintaining continuity at the boundaries. This can be achieved directly through local evaluation of the normal (to the boundary) component of the velocity when the perpendicular components are zero gradient or constant, for example, as adopted in this work. Furthermore, the pressure term must be evaluated in a consistent manner on the normal velocity boundary. If a Neumann boundary condition is adopted then the pressure must be defined as a Dirichlet boundary condition, otherwise the boundary is underspecified. The converse is required

for accuracy but not for stability. On the side boundaries of the computational domain it was assumed that the flow could only enter the domain, and at the top of the domain the flow was assumed to only exit. When these conditions were not met then the local velocity was clipped to zero and the appropriate pressure boundary applied.

The fractional step method of Najm et al. [36] was employed. Since the density difference is less than unity, only the first step is required whilst maintaining second order accuracy in time. The convective terms were discretised such that a true laminar (or instantaneous) simulation could be run, i.e. one without a subgrid model. A third order upwind scheme was implemented for the momentum convection terms, and a second order TVD scheme 'superbee' was implemented for the temperature convection terms.

Following Zhou et al. [15], the inlet velocity boundary condition forced instabilities imposed to ensure a sufficiently rapid transition. These were twofold. Firstly, random fluctuations of random duration with a maximum value of 0.35 and maximum duration of 200 time steps for each velocity component. Secondly, the structured instability of Menon and Rizk [37], given by Eq. (4.1), was employed.

$$v' = AV(r)\sum_{n=1}^{2}\sin(2\pi ft/n+\theta) \qquad (4.1)$$

A is the fraction of the inlet velocity, 0.2, $V(r)$ is the inlet velocity as a function of radius, f is the frequency constant, 0.3, t is the time, and θ is the angle from the centre of the source.

The simulations were run for 50,000 time-steps of 0.012s, with appropriate average values being obtained over the last 35,000 time-steps.

5. Results

It is often stated that for engineering applications the choice of LES model will not affect the overall result. This is shown not to be the case, although the models do have more or less effect.

Code validation is carried out on laminar buoyant jets and turbulent non-buoyant jets in [38]. The grid used is too coarse to accurately handle the rapid transition to full turbulence. A coarse grid simulation [38] indicates the sensitivity of the near-field to the grid resolution, and also that the resolution is sufficient for the fully developed turbulent region. Fixed mesh refinement and adaptive mesh refinement techniques are presently being coded which will help overcome this deficiency. The coarseness of the grid is essential for the LES models to be useful however, since the more refined the grid is, the less energy is in the subgrid scales, and hence the less important are the LES models.

The focus of this work is on the relative behaviour of the models and their mechanics rather than their comparison with the experimental data, for which the simulations carried out do not provide appropriate data, since the region of self-similarity, although observable, does not cover a great enough region to extract useful spread-rate information.

Figure 1 and figure 2 show the turbulent kinetic energy spectrum (TKE) and temperature fluctuation spectrum (TFS) respectively. The usual -5/3 gradient is achieved for the TKE, and also for the TFS, but the required -3 gradient at smaller scales [12] is not found, due to the relative coarseness of the grid.

The models being reviewed are considered in subgroups. The eddy stress models are considered first. These are all qualitatively the same, although with clearly differing results. The centerline values for mean velocity and temperature provide the largest scale comparisons and the graph of the vertical velocity component (figure 3) shows the difference in magnitude very clearly. The similarity between the models is indicated with the vertical normal stresses, τ_{22} in figure 4, along the centerline. The structure function model is the most dissipative, as indicated by the slower transition (which starts at approximately 4 diameters from the inflow boundary), and the faster decay, followed by the one equation model, and finally the Smagorinsky and buoyancy-modified-

Smagorinsky models. The decay for a simulation without a sub-grid model is also plotted, and is observably less than for any of the other models.

Notably the Smagorinsky and buoyancy-modified Smagorinsky models give almost identical results contrary to the findings of [4], who find the buoyancy-modified version less accurate than the standard Smagorinksy model. The formulation used here is slightly different, however, in that the turbulent viscosity is evaluated from the square root of the absolute value given in Eq. (3.4), and not fixed to zero when the root is imaginary.

The eddy models here are qualitatively almost similar (apart from the one equation model near the inlet, where the method has not given the model sufficient time and distance to evaluate the turbulent kinetic energy properly). The adjustment of the model constants could make the models almost identical, due to the similarity.

These models all break the realizability conditions [39, 40], which are necessary when the top-hat filter is used. This is clear, since the formulation considers the gradient in the normal stresses also which can be either positive or negative (to satisfy the realizability conditions these stresses must always be positive). This is also demonstrated in figure 4.

The flux eddy models (the SGDH with a turbulent Prandtl number of 0.4, and the GGDH models with a constant of 5, an order of magnitude higher than that used for the RANS model analogue) show the flux to be the dominant term in the effect on the overall decay. The GGDH models are much faster to go through transition (due to their extra complexity, the dissipation is evaluated considering gradients in all three axes, and hence does not recognize the edge of the laminar jet as turbulence so strongly). The centerline decays are shown in figure 5. The qualitative behavior of the GGDH models is a distinct improvement on the SGDH model, but the different formulations have different magnitudes of flux values. The constants for these models need to be better evaluated (as does the constant for the SGDH model still), but these are promising.

More important however, is the simulation without a flux model, only using the stress model, also plotted in figure 5. This used the one equation model for the stresses. The decay rate was brought

almost to the point of no model being used at all, even though in conjunction with the SGDH model, this was the second most dissipative model. This shows the importance of the interaction between the models (since the flux eddy models are dependent on the turbulent viscosity as calculated by the stress model), and the importance of consideration of the flow to be simulated. The Bardina and Leonard models are termed the structure models (the structure function model is an eddy model) both for the stresses and fluxes. It was impossible to test the structure models independently with the same conditions; they were found to be unstable, but when mixed with an eddy stress or eddy flux model, they were stable. The resultant simulations deviated very little from the centerlines of the non-subgrid model simulation due to a cancellation of the effects of the structure and eddy components, confirmed in the dynamic model results. These two models, qualitatively the same as each other, are distinctly different from the eddy models. This is appropriate though, since generally speaking, the eddy models are most suitable to model the Reynolds terms, and possibly the Cross terms, whereas the structure models are most representative of the Leonard terms and possibly the Cross terms. In this light, the lack of stability makes sense for the structure models used by themselves, since there is no term to dissipate the energy building up in the small scales. Both adhere to the realizability conditions (although the Leonard model would not if the Kwak (equation 3.14) variant was used, since it does not square the terms), ensuring their lack of similarity with the eddy model.

The structure models stresses are significantly larger than the eddy model stresses, figure 6, and have different dominant terms. For the eddy models the radial/axial stresses, τ_{12}, τ_{23}, and their symmetric equivalents, are dominant, whereas the axial stresses are dominant for the structure models. This is obviously particular to the buoyant jet situation, but highlights the significant differences between the two types of model. Also the radial normal stresses are larger than the cross stresses for the structure models. Worthy [38] goes into more detail on this.

The dynamic Smagorinsky and LDM models give centerline values the same as a simulation without a subgrid model. The 'internal' properties of the models are considered, although the results are somewhat skewed due to the amount of dissipation provided by the upwind and TVD convective schemes. All of the dynamic models have the very important quality of having zero turbulent viscosities in the laminar regions and are weaker than their static counterparts in the transitional region, shown in figure 7. Figure 8 shows the τ_{22} centerlines, from which the inversion of the relative magnitudes can be seen. Although the turbulent viscosity of the dynamic models is lower on average, the stress is larger. This possibly indicates a correlation of the clipping to the direction of the gradient of the velocity.

The average value of the Smagorinsky constant is plotted along the centerline in figure 9, and can be seen to take a value of approximately 0.008, only slightly below the usual value of 0.01, and the numerical scheme gives a good explanation of this. The model constants for LDM simulations are found much below the recommended value of 0.07, estimating 0.02 in the fully turbulent region. This value is found regardless of the strength of the subgrid kinetic energy used in the model constants' evaluation. Figure 10 shows the different SKE centerlines depending on whether dynamic procedures were used in the SKE transport equation. Jiminez [41] suggests that the dynamic procedure adjusts itself to dissipate the necessary amount of energy. The implication here is that the model constant is not dependent on where in the inertial range the filter is, which is a positive result. The differences in the LDM SKE levels is clearly attributable to the dynamic procedures applied in the transport equation. The dissipation term is modeled well, with an average constant between 2.5 and 3 in the turbulent region, higher than the recommended value of 1. The diffusion term, not modeled at all by Davidson [26] since it was considered an insignificant term, was modeled poorly, with the constant varying to a maximum of above 100, and an average two orders of magnitude different from the recommended 0.1. Nevertheless the

variation of the diffusive term did correspond well to the flow (i.e. low in the laminar regions higher in the turbulent regions, and maximum in the region of forced instability at the inflow). The dynamic SGDH model takes negligible values for the fluxes. There were two immediate possible reasons, that the TVD scheme has already dissipated enough thermal energy, or that the thermal turbulent fluctuations were not in synchronization with the turbulent kinetic energy fluctuations. Simulations using a third order upwind scheme instead of the second order TVD scheme gave similar results, and so the first possibility was dismissed. The latter remains a possibility, and dynamic flux models in which the turbulent viscosity does not depend on the dynamic stress model constant could overcome this. The same problem is encountered with the dynamic GGDH models.

Table 1 shows the percentage of non-clipped constants at a couple of points along the centerline. It shows that the level of clipping for the dynamic SGDH model is not low enough to explain the shortfall of the model constant. The Smagorinsky model achieves a healthy 68% calculated. The percentages from the dynamic mixed model simulations are also given. The expectation was that with the structure model handling the backscatter and the large subgrid-scale transfer the Smagorinsky component constant would be clipped less. This is not the case – the behaviour of the Smagorinsky model appears to be largely unaffected, although the constant does double in value, canceling out the effect of halving in the type 1 formulation of the mixed model.

Figure 11 shows the velocity decays of the mixed models. The accelerated transition can clearly be seen, further showing the opposite effect of the eddy and structure components. The dynamic procedure still maintains the eddy component at near zero through the transitional period, while the structure component already is a significant term. This suggests the dynamic mixed models are the most accurate of the models considered here for the stresses, although the computational cost has not been mentioned and is considerably more in both operation count and memory requirements.

6. Conclusion

This work has investigated both the relative effect on the outcome of the averaged results and also the mechanics of the different models on a buoyant jet.

The main conclusion is that in a buoyant transitional flow the choice of LES model can have a significant impact. In the stress models the eddy models and the 'structural' models – that is the Leonard and Bardina models – have opposite effects on the transition point, with the 'structural' models aiding transition while the eddy models delay it. For the flux models the GGDH models greater complexity does indeed appear to give it an advantage over the SGDH model, although the model constant needs to be better established (although this is still true of the SGDH model). The difference in the static eddy models is significant, although since they are qualitatively similar, an adjustment in the model constant should make them equivalent.

A number of observations about the dynamic models are made. It has been long known that dynamic modeling with an eddy model is unstable if backscatter is allowed to be larger than the molecular viscosity [27]. Here the percentage of clipping in the turbulent regime is similar but less than that found by Piomelli et al. [42] in non-buoyant channel flow. The hope that the dynamic mixed modelling would reduce the amount of clipping was not rewarded, indicating that the eddy model is, in effect, acting on the larger subgrid scales as well as the smaller, which is only a desirable feature when the 'structural' model is not included to represent these terms.

The dynamic modeling of the flux terms was very poor, with negligible values being attained, and further investigation into this is required. Mixed modeling did not improve the situation (in terms of the eddy component).

The dynamic one equation model or 'localized dynamic model' has significant internal differences dependent on the modeling method for the subgrid kinetic energy transport terms, but in these simulations do not show significant differences in the outcome of the simulations. The constant of dissipation was found to be underestimated, with the dynamic procedure estimating it to be approximately three times the usually prescribed value (although note this value is based on

averaging which includes the zeros of clipped values). The dissipation terms were modeled highly erratically and a static model for these terms is suggested.

The final recommendation for choice of LES model would be a dynamic mixed model for the stresses and the static GGDH model for the fluxes, although for a rapid simulation the stability considerations of upwind or TVD schemes (without subgrid model) may outweigh the requirement of better accuracy.

References

1. Lilly, D. K., On the numerical simulation of buoyant convection, Tellus, XIV(2), p144, 1962.

2. Smagorinsky, J., General circulation experiments with the primitive equations, Mon. Weather Rev., 91, p99, 1963.

3. Germano, M., Turbulence: the filtering approach, J. Fluid Mech., 238, p325, 1992.

4. Bastiaans, R., J. M., Rindt, C. C. M., Nieuwstadtadt, F. T. M. and van Steenhoven, A. A., Direct and large-eddy simulation of the transition of two- and three-dimensional plumes in a confined enclosure, I. J. Heat Mass Trans., 43, p2375, 2000.

5. Bastiaans, R., J. M., Rindt, C. C. M. and van Steenhoven, A. A., Experimental analysis of a confined transittional plume with respect to subgrid-scale modelling, Int.. J. Heat & Mass Transfer, 41, p3989, 1998.

6. Basu, A. J. and Mansour, N. N., Large eddy simulation of a forced round turbulent buoyant plume in neutral surroundings, Annual Research Briefs, Centre for Turbulence Research, NASA Ames/Stanford Univ., 1999.

7. Webb, A. T. and Mansour N. N., Towards LES of jets and plumes, Annual Research Briefs, Centre for Turbulence Research, NASA Ames/Stanford Univ., 2000.

8. Paulucci, S., On the Filtering of Sound from the Navier-Stokes Equations, Sandia National Labs, Report SAND-82-8257, 1982.

9. Rehm, R. G. and Baum, H. R., The Equations of Motion for Thermally Driven, Buoyant Flows, J. Res. Nat. Bur. Stand., 83, p297, 1978.

10. Leonard, A., Energy cascade in large-eddy simulations of turbulent flows, Adv. Geophys., 18, p237, 1974.

11. Piomelli, U., Large Eddy Simulation: Achievements and Challenges, Progress in Aerospace Sciences, 35, p335, 1999.

12. Schumann, U., Subgrid-scale model for finite-difference simulations in plane channels and annuli, J. Comp. Phys., 18, p376, 1975.

13. Sagaut, P., Large Eddy Simulation for Incompressible Flows: An Introduction, Springer-Verlag, Berlin, 2000.

14. Lilly, D. K., A proposed modification of the Germano subgrid-scale closure method, Phys. Fluids A, 4(3), p633, 1992.

15. Zhou, X., Luo, K. H., and Williams, J. J. R., Large-eddy simulation of a turbulent forced plume, Eur. J. Mech. B – Fluids, 20, p233, 2001.

16. Metais, O. and Lesieur, M., Spectral large eddy simulations of isotropic and stably-stratified turbulence, J. Fluid Mech., 239, p157, 1992.

17. Lesieur, M. and Metais, O., New Trends in Large Eddy Simulation, Ann. Rev. Fluid Mech., 28, p45, 1996.

18. Schmidt H., and Schumann, U., Coherent Structure of the Convective Boundary Layer Derived from Large-Eddy Simulations, J. Fl. Mech., 200, p511, 1989.

19. Sanderson, V. E., Turbulence Modelling of Turbulent Buoyant Jets and Compartment Fires, PhD Thesis, Cranfield University, 2001.

20. Worthy, J., Sanderson, V., and Rubini, P. A., Comparison of Modified k-ε Turbulence Models for Buoyant Plumes, Num. Heat Transfer, Part B, 39, p151, 2001.

21. Daly, B. J., and Harlow, F. H., Transport Equations in Turbulence, Phys. Fluids, 13(11), p2634, 1970.

22. Bardina, J., Ferziger, J. H., and Reynolds, W. C., Improved subgrid scale models for large eddy simulations, AIAA paper No. 80-1357.

23. Kwak, D., Reynolds, W. C., and Ferziger, J. H., Numerical Simulation of Turbulent Flow, Thermosciences Division. Dept. Mech. Eng., Stanford University, Report No. TF-5, 1975.

24. Germano, M., Piomelli, U., Moin, P., and Cabot, W. H., A dynamic subgrid-scale eddy viscosity model, Phys. Fluids A, 3(7), p1760, 1991.

25. Piomelli, U., and Liu, J., Large-eddy simulation of rotating channel flows using a localized dynamic model, Phys. Fluids, 7(4) , p839, 1995.

26. Davidson, Lars, Large Eddy Simulation: A Dynamic One-Equation Subgrid Model for Three-Dimensional Recirculating Flow, 11th Int. Symp. on Turb. Shear Flow, Vol. 3, p26.1, Grenoble, 1997.

27. Lund, T. S., Ghosal, S., and Moin, P., Numerical experiments with highly variable eddy viscosity models, in Engineering Applications of Large Eddy Simulation, eds. Ragale, S. A., & Piomelli, U., FED Vol. 162, ASME, 1993.

28. Balaras, E., and Benocci, C., Large eddy simulations of flow in a square duct, Proc. Of the thirteenth symposium on turbulence, Univ. of Missouri Rolla, 1992.

29. Zang, Y., Street, R. L., and Koseff, J. R., A dynamic mixed subgrid-scale model and its application to turbulent recirculating flows, Phys. Fluids A, 5(12), p3186, 1993.

30. Vreman, B., Guerts, B., and Kuerten, H., On the formulation of the dynamic mixed subgrid-scale model, Phys. Fluids, 6(12), p4057, 1994.

31. Wong, V. C., A proposed statistical-dynamic closure method for the linear or nonlinear subgrid-scale stresses, Phys. Fluids A, 4(5), 1992.

32. Ghosal, S., Lund, T. S., Moin, P., and Akselvoll, K., A dynamic localization model for large-eddy simulation of turbulent flows, J. Fluid Mech., 286, p229, 1995.

33. Kim,W.-W., and Menon, S., A New Dynamic One Equation Subgrid Model for Large Eddy Simulations, 33rd Aerospace Sciences Meeting, AIAA Paper No. 95-0379, Reno, NV, Jan 9-12, 1995.

34. Shabbir, A. and George, W. K., Experiments on a round turbulent buoyant plume, J. Fluid. Mech., 275, p1, 1994.

35. Gresho, P. M., Incompressible Fluid Dynamics: Some Fundamental Formulation Issues, Ann. Rev. Fluid Mech., 23, p413, 1991.

36. Najm, H.N., Wyckoff, P.S., and Knio, O..M., A Semi-Implicit Numerical Scheme for Reacting Flow. I. Stiff Chemistry, J. Comp. Phys., 143(2), p381, 1998.

37. Menon, S. and Rizk, M., Large Eddy Simulations of Three-Dimensional Impinging Jets, Int. J. Comp. Fl. Dyn., Vol. 7, p275, 1996.

38. Worthy, J., Large Eddy Simulation of Buoyant Plumes, PhD Thesis, Cranfield University, 2003.

39. Schumann, U., Realizability of Reynolds-stress turbulence models, Phys. Fluids, 20(5), p721, 1977.

40. Vreman, B., Guerts, B., and Kuerten, H., Realizability conditions for the turbulent stress tensor in large-eddy simulation, J. Fluid Mech., 278, p351, 1994.

41. Jimenez, J., On why dynamic subgrid-scale models work, Annual Research Briefs, Centre for Turbulence Research, NASA Ames/Stanford Univ., 1995.

42. Piomelli, U., Moin, P., and Ferziger, J., Large Eddy Simulation of the Flow in a Transpired Channel, AIAA Report 89-0375, 1989.

Appendix A

We follow Ghosal et al. [32] for the dynamic evaluation of the SKE transport equation terms. Similarly to the usual dynamic procedure, use of a test filtered subgrid kinetic energy transport equation is considered.

$$TRANS(k) = P_k - C_1 \frac{k^{3/2}}{\overline{\Delta}} + C_2 \frac{\partial}{\partial x_j}(\overline{\Delta} k^{1/2} \frac{\partial k}{\partial x_j}) + B_k \qquad \text{A.1}$$

$$TRANS(K) = P_K - C_1 \frac{K^{3/2}}{\overline{\Delta}} + C_2 \frac{\partial}{\partial x_j}(\overline{\Delta} K^{1/2} \frac{\partial K}{\partial x_j}) + B_K \qquad \text{A.2}$$

The two constants can now be dynamically calculated (if the buoyant production term has an unknown constant this can be evaluated dynamically before this procedure is used, although this is not done here-the static SGDH model is used).

C_2 is attained with the following. Let

$$Z_j \equiv \overleftrightarrow{\overline{u}}_j \overleftrightarrow{(\overline{p} + k + \overline{u}_i \overline{u}_i / 2)} - \overleftrightarrow{\overline{u}_j (\overline{p} + k + \overline{u}_i \overline{u}_i / 2)} \qquad \text{A.3}$$

Note that the two terms on the rhs of Eq. (A.3) are the exact terms that are being modeled (before the differential operator is applied).

$$C_2^{n+1} = (Z_j + \overline{\Delta} \overleftrightarrow{C_2^n k^{1/2} \frac{\partial k}{\partial x_j}})(\overleftrightarrow{\overline{\Delta}} K^{1/2} \frac{\partial K}{\partial x_j})^{-1} \qquad \text{A.4}$$

C_1 can now be calculated by substituting Eq. (A.4) into Eq. (A.1), filtering and equating it with Eq. (A.2).

$$C_1^{n+1} = (\overleftrightarrow{P_k} + P_K + \frac{\partial \overleftrightarrow{f_j}}{\partial x_j} + \frac{\partial F_j}{\partial x_j} + \overleftrightarrow{B}_k + B_K + \overleftrightarrow{C_1^{n+1} \frac{k^{3/2}}{\overline{\Delta}}}) / (\frac{K^{3/2}}{\overleftrightarrow{\overline{\Delta}}}) \qquad \text{A.5}$$

Davidson's [26] formulation lets $C_2 = 0$, assuming it is a negligible term. This also simplifies the evaluation of C_1.

The subgrid energies must not be allowed to become negative, which is achieved with clipping.

Percentage of Used Dynamic Constants

	d2f		d1m	d2m	
y/D	C	C_SGDH	C	C	C_SGDH
7.11	66%	50%	63%	61%	36%
10.66	68%	57%	72%	68%	30%

Table 1. Percentage of dynamically evaluated constants not clipped.

Figure Captions

Figure 1. Turbulent kinetic energy spectra plot for structure function model simulation, s1f, at y/D=10.66.

Figure 2. Temperature fluctuations spectra, TT(k), for structure function model simulation, s1f, using SGDH for the fluxes, at y/D=10.66.

Figure 3. Velocity centrelines for d1n, no subgrid model, s1t, Smagorinsky model, s2t, buoyancy-modified Smagorinsky model, s1f, structure function model, o1e, one equation model.

Figure 4. T22 centrelines for s1t, Smagorinsky model, s2t, buoyancy-modified Smagorinsky model, s1f, structure function model, o1e, one equation model.

Figure 5. Vertical velocity centrelines for d1n, no subgrid model, o1e, one equation model with SGDH flux, o2e, one equation stress model, no flux model, f1c, one equation model with first formulation of the GGDH model, GGDH_1, f2c, one equation model with second formulation of the GGDH model, GGDH_2.

Figure 6. Vertical normal stress, T22, centrelines for s1t, Smagorinsky model and SGDH flux, m1x, mixed Smagorinsky/Bardina stress model, mixed SGDH Bardina flux model, m2x, mixed Smagorinsky/Leonard stress model, no flux model.

Figure 7. Turbulent viscosity centrelines for s1t, static Smagorinsky stress and static SGDH flux models, d1f, dynamic Smagorinsky stress, static SGDH flux models, d2f, the dynamic Smagorinsky stress and dynamic SGDH flux models.

Figure 8. T22 centrelines for s1t, static Smagorinsky stress and static SGDH flux models, d1f, dynamic Smagorinsky stress, static SGDH flux models, d2f, the dynamic Smagorinsky stress and dynamic SGDH flux models.

Figure 9. Smagorinsky constant centrelines for d1f, dynamic Smagorinsky stress, static SGDH flux models, d2f, the dynamic Smagorinsky stress and dynamic SGDH flux models.

Figure 10. Subgrid kinetic energy centrelines for l1d, LDM with dynamic SKE constants stress, static SGDH flux models, l2d LDM with static SKE constants stress, static SGDH flux models.

Figure 11. Velocity centrelines for d1n, no subgrid models, d1f, dynamic Smagorinsky stress and static SGDH flux models, d1m, dynamic Smagorinsky/ Bardina stress and static SGDH flux models, d2m, dynamic Smagorinsky/ Bardina stress and dynamic SGDH/ Bardina flux models.

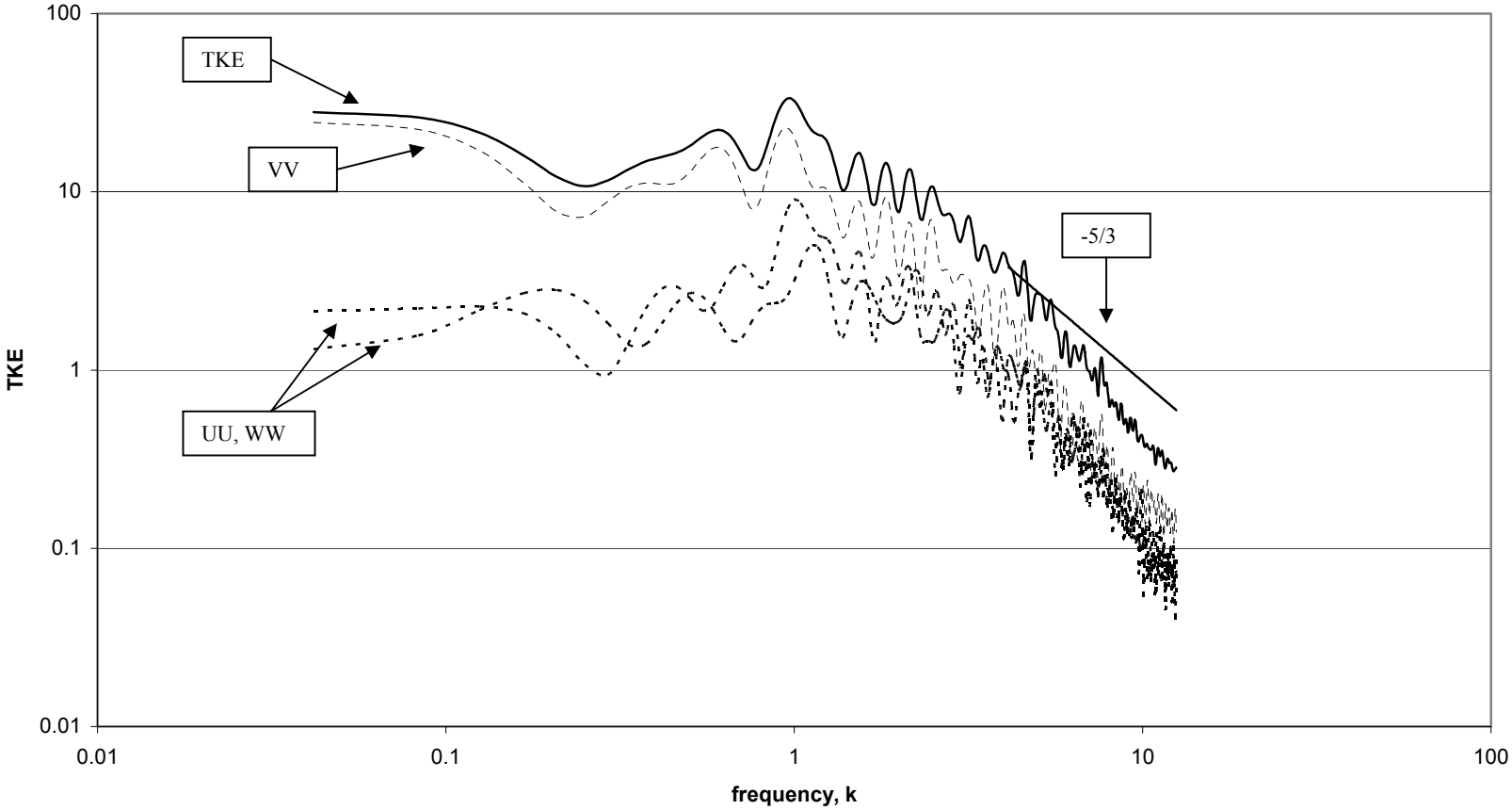
s1f - TKE Time Spectra y/D=10.66
TKE
VV
UU, WW
-5/3
100
10
1
0.1
0.01
TKE
0.01
0.1
1
10
100
frequency, k

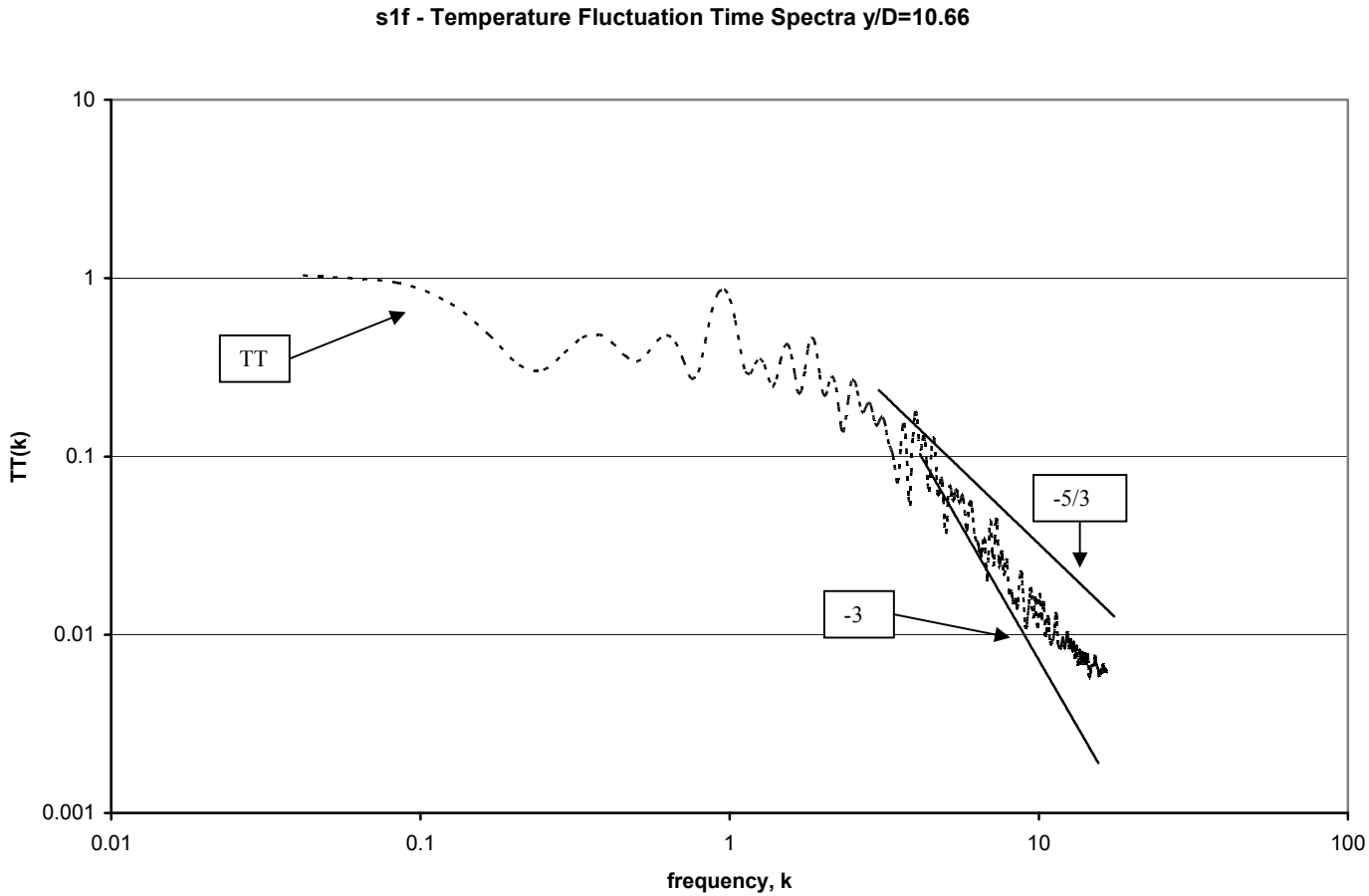
s1f - Temperature Fluctuation Time Spectra y/D=10.66
10
1
0.1
0.01
0.001
TT(k)
TT
-5/3
-3
0.01
0.1
1
10
100
frequency, k

.

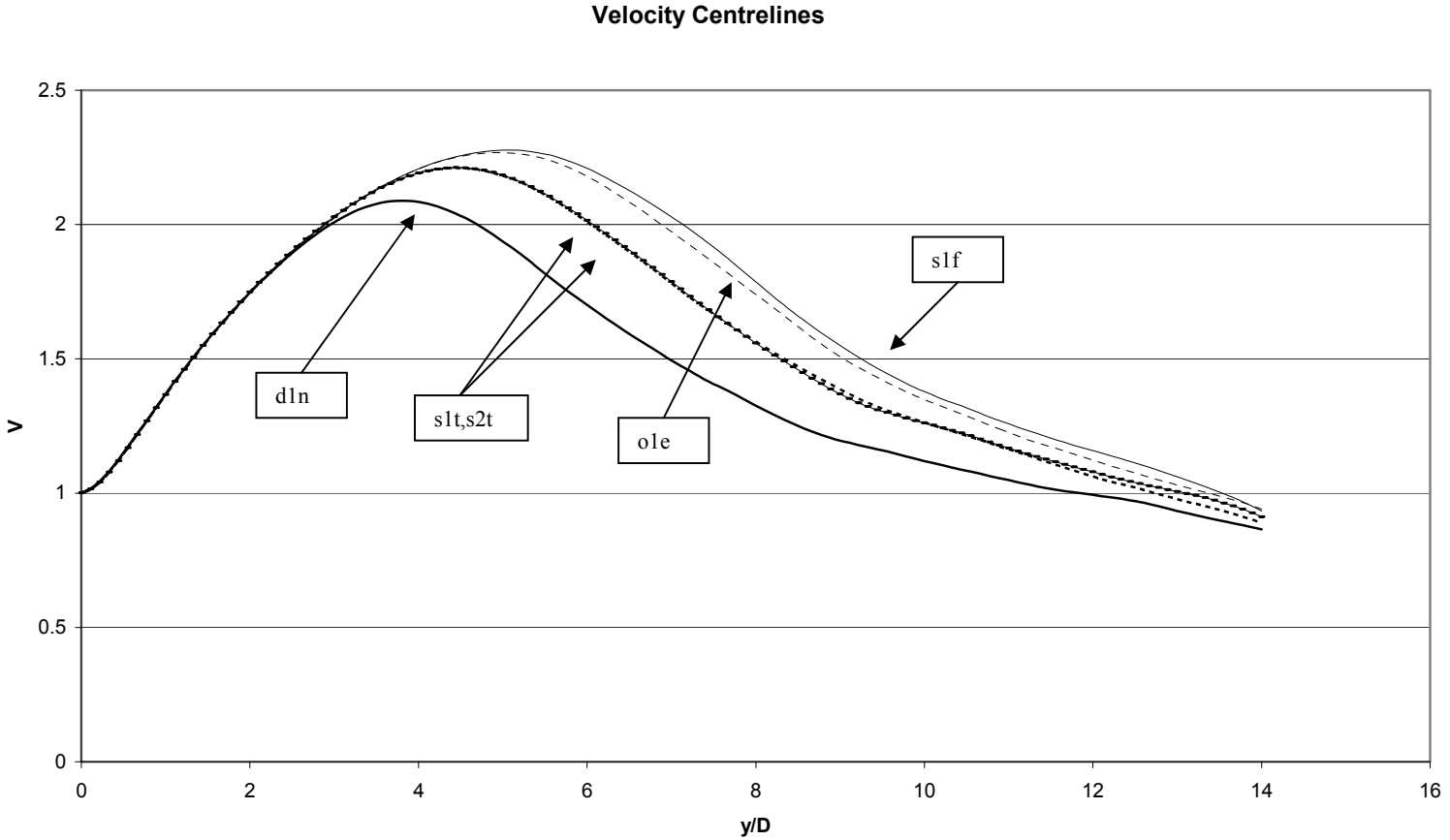
Velocity Centrelines
2.5
2
1.5
1
0.5
0
V
0
2
4
6
8
10
12
14
16
y/D
d1n
s1t,s2t
o1e
s1f

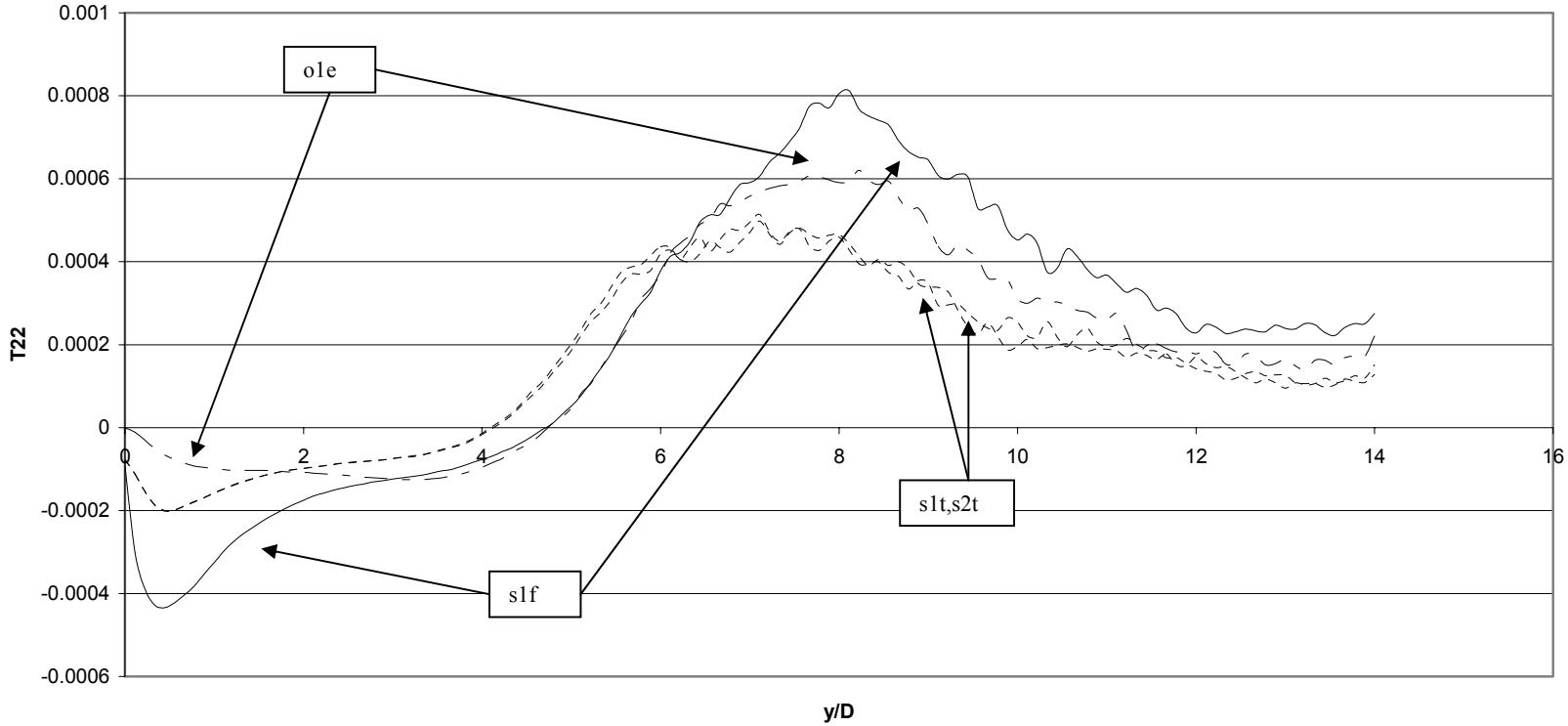
T22 Centrelines
0.001
0.0008
0.0006
0.0004
0.0002
0
-0.0002
-0.0004
-0.0006
T22
0
2
4
6
8
10
12
14
16
y/D
o1e
s1t,s2t
s1f

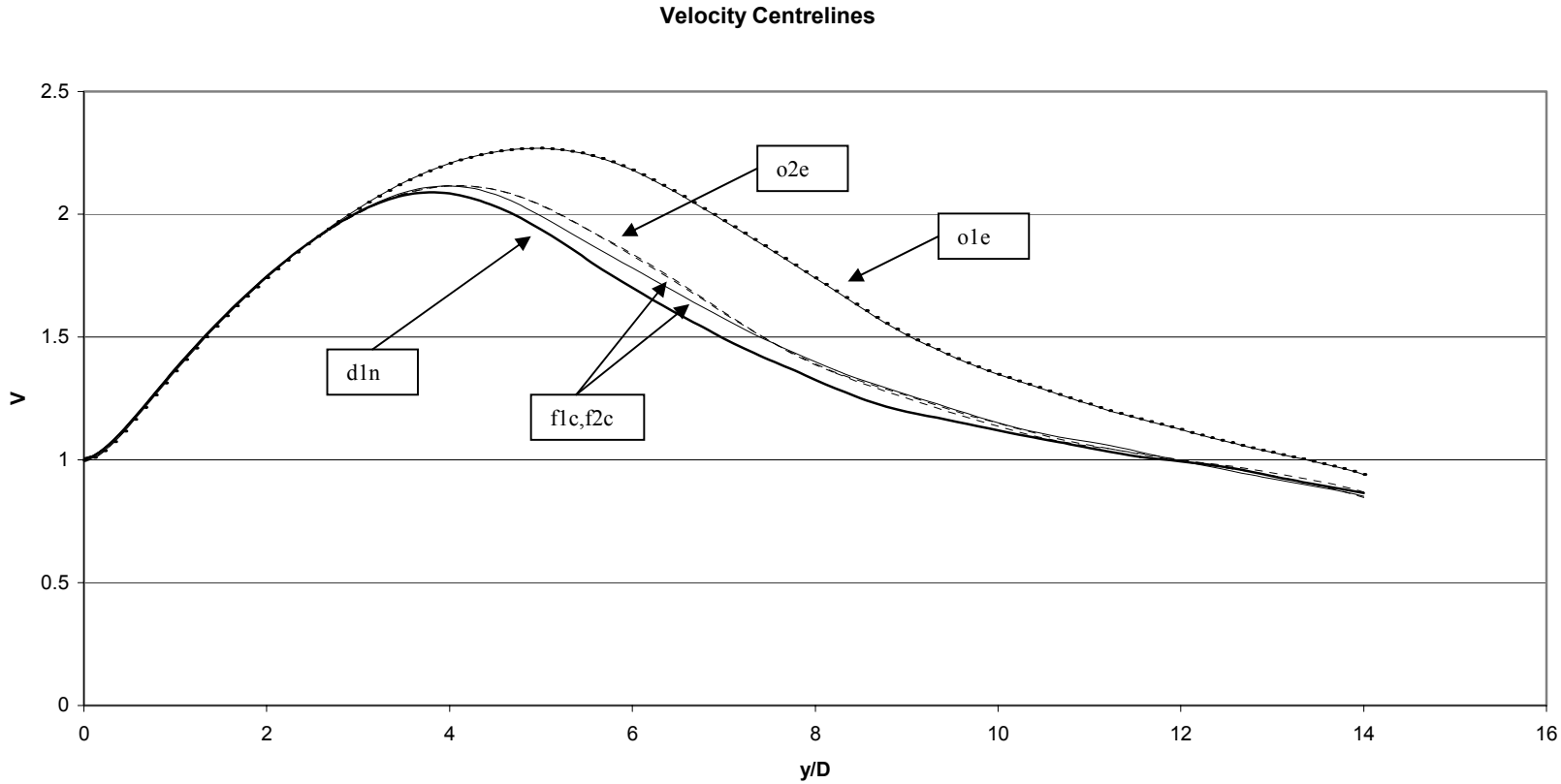
Velocity Centrelines
2.5
2
1.5
1
0.5
0
V
0
2
4
6
8
10
12
14
16
y/D
o2e
o1e
d1n
f1c,f2c

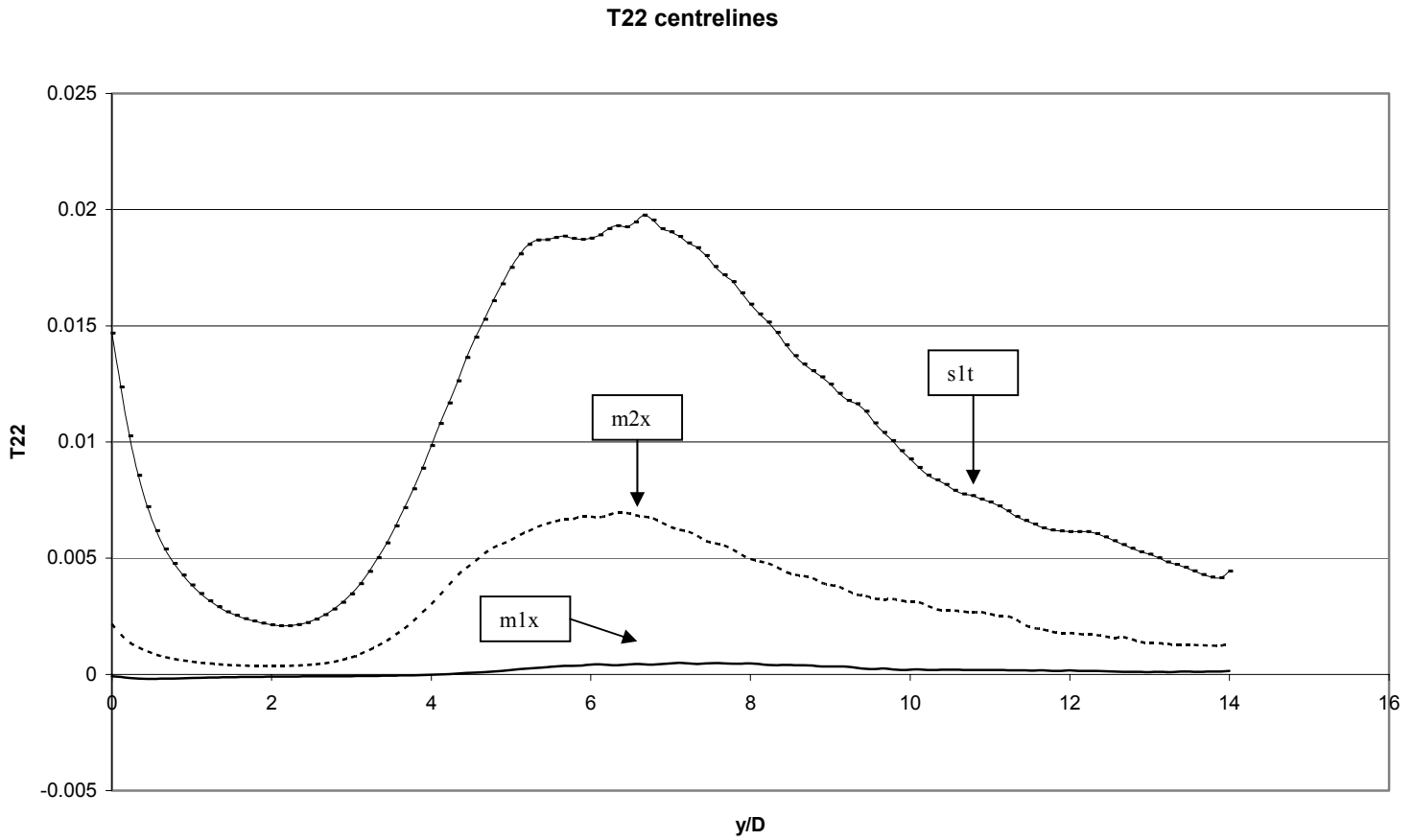
T22 centrelines
0.025
0.02
0.015
0.01
0.005
0
-0.005
T22
0
2
4
6
8
10
12
14
16
y/D
s1t
m2x
m1x

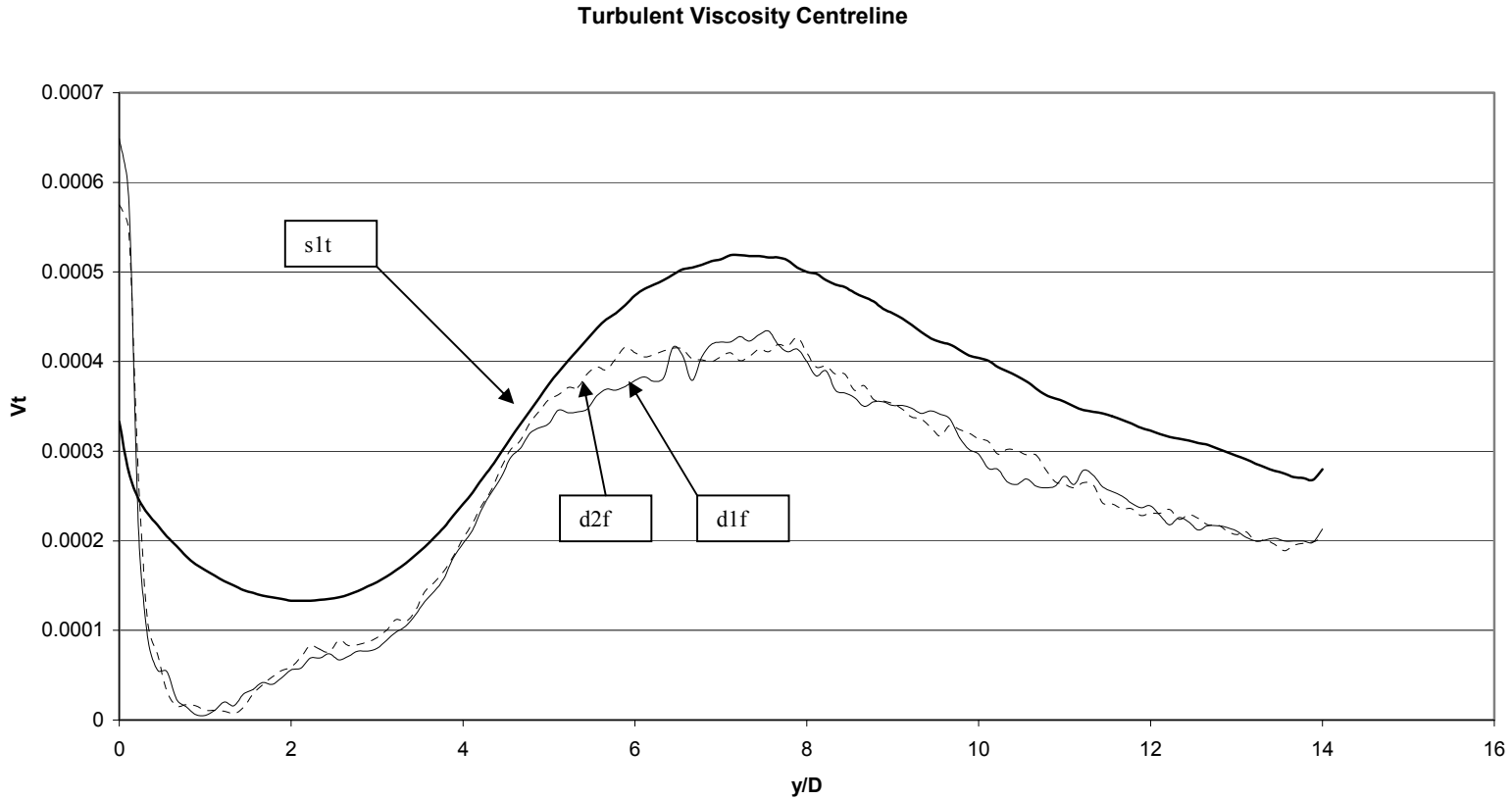
Turbulent Viscosity Centreline
0.0007
0.0006
0.0005
0.0004
0.0003
0.0002
0.0001
0
Vt
s1t
d2f
d1f
0
2
4
6
8
10
12
14
16
y/D

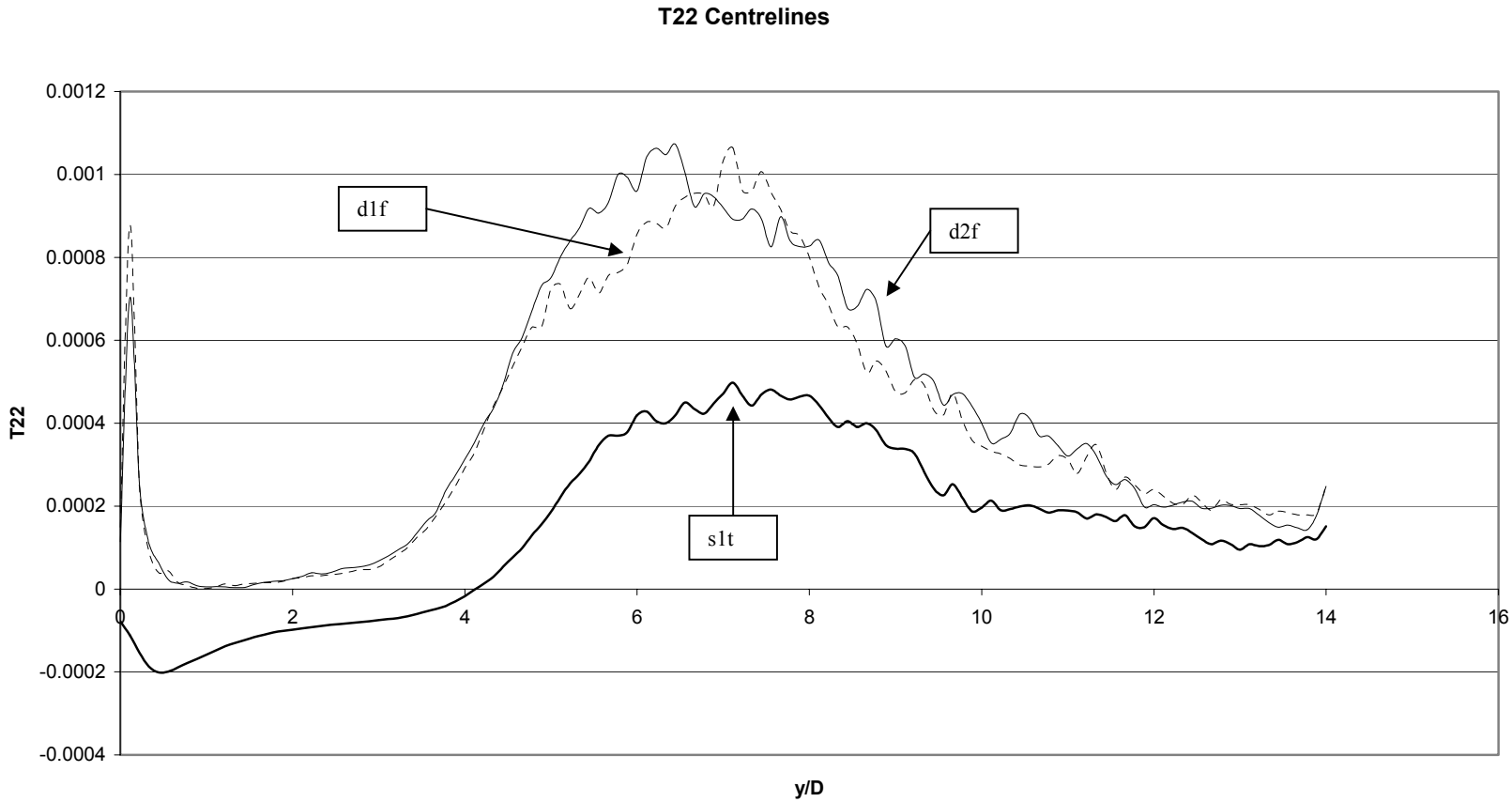
T22 Centrelines
0.0012
0.001
0.0008
0.0006
0.0004
0.0002
0
-0.0002
-0.0004
T22
0
2
4
6
8
10
12
14
16
y/D
d1f
d2f
s1t

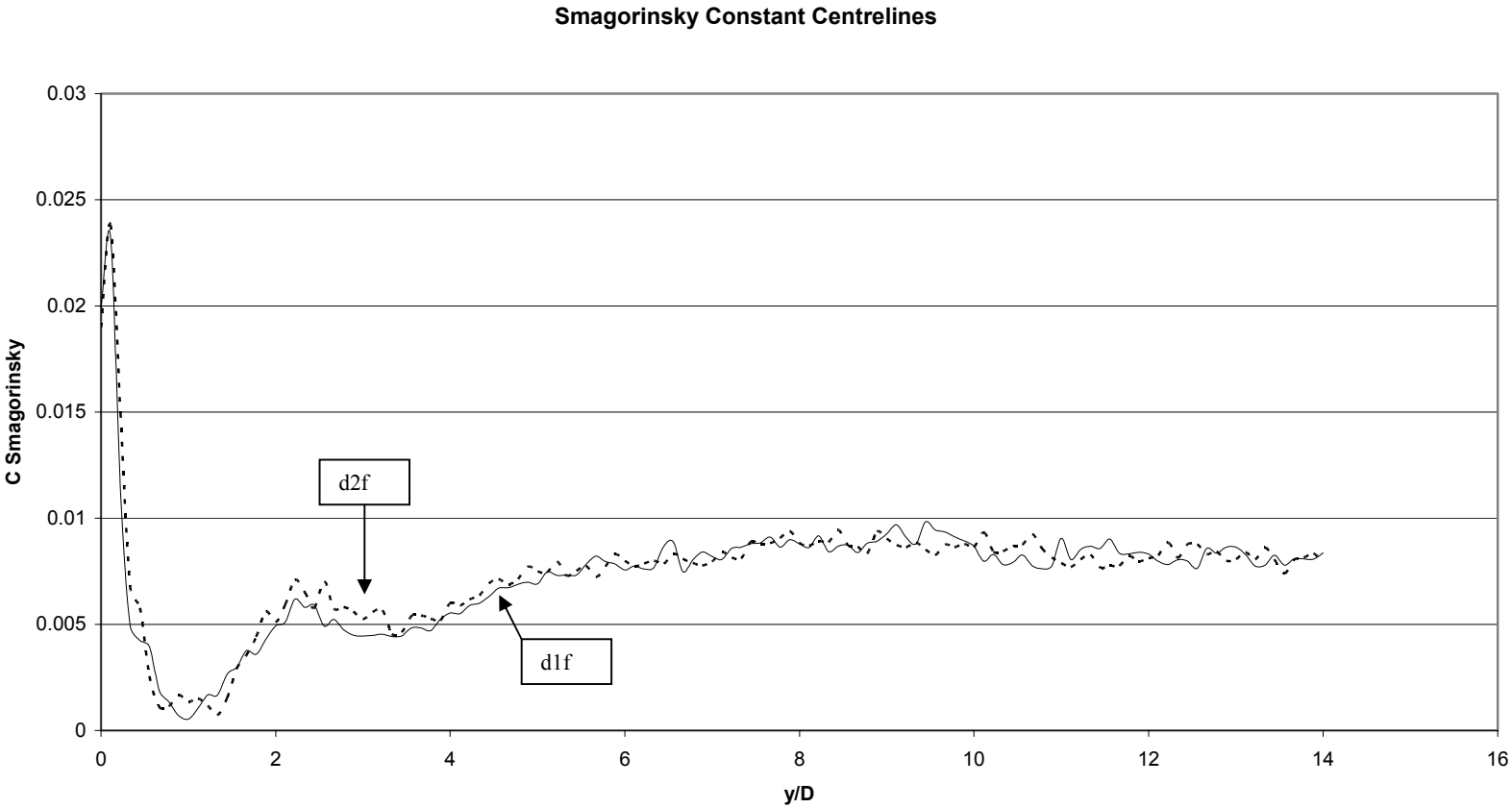
Smagorinsky Constant Centrelines
C Smagorinsky
0.03
0.025
0.02
0.015
0.01
0.005
0
0
2
4
6
8
10
12
14
16
y/D
d2f
d1f

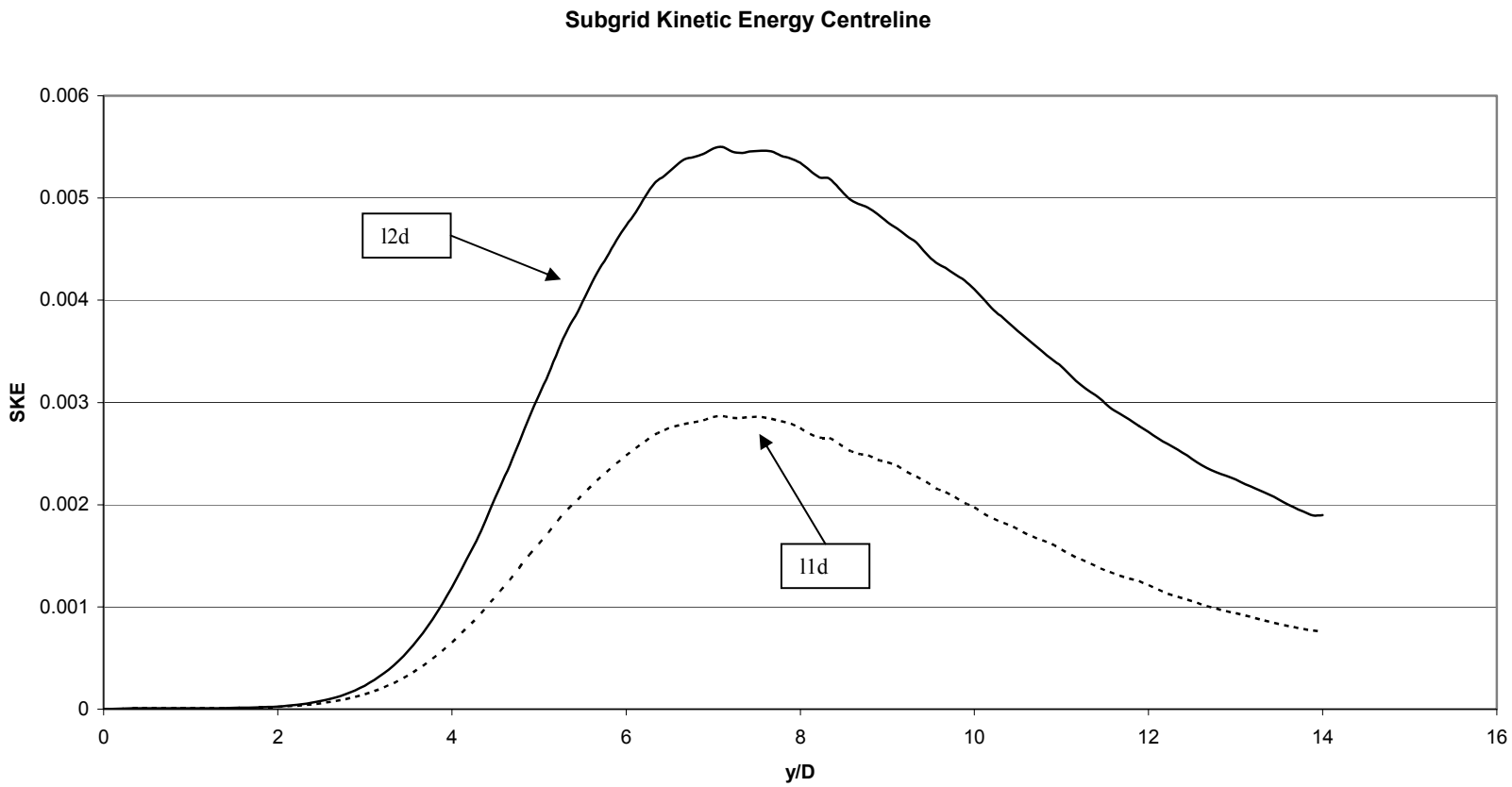
Subgrid Kinetic Energy Centreline
0.006
0.005
0.004
0.003
0.002
0.001
0
SKE
l2d
l1d
0
2
4
6
8
10
12
14
16
y/D

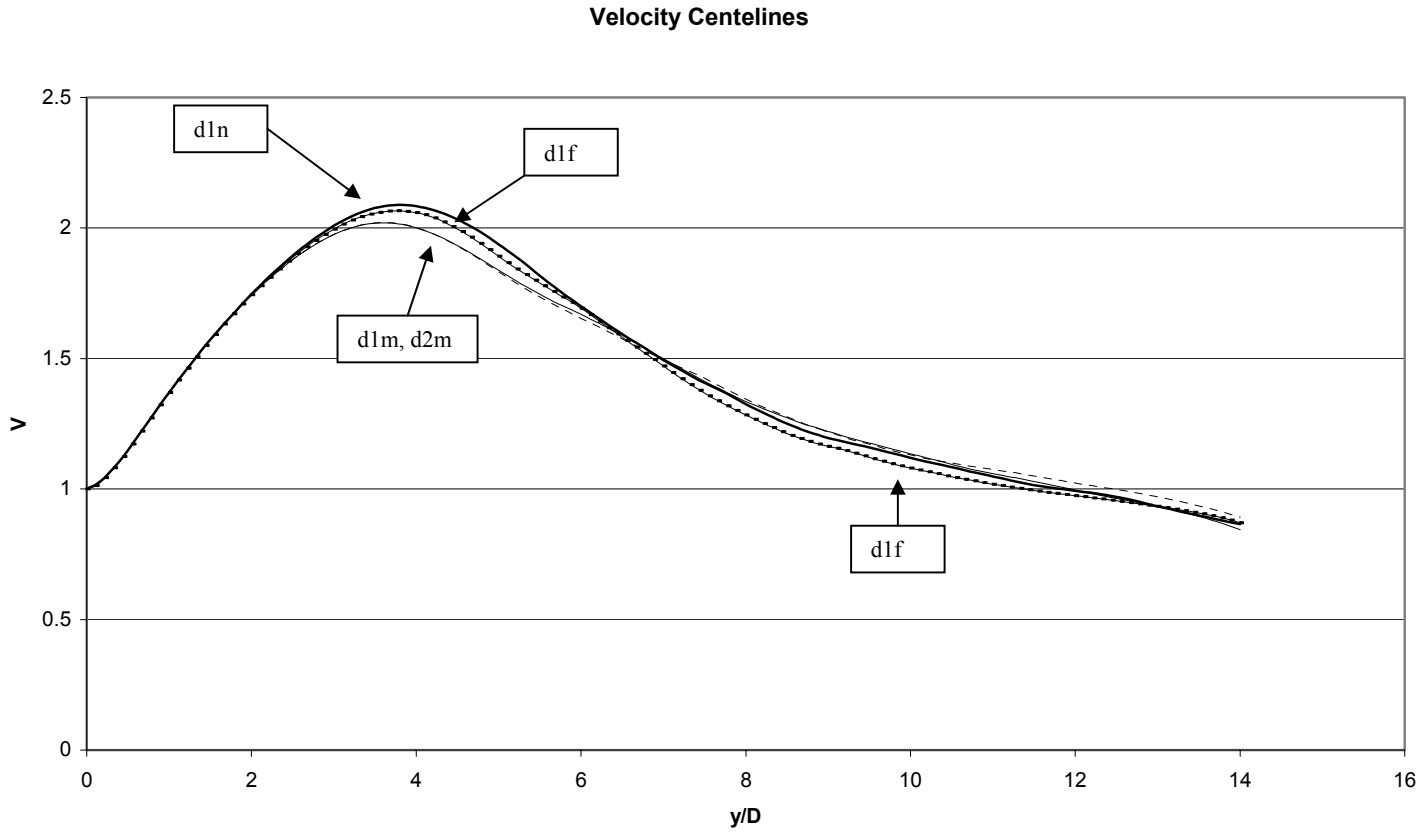
Velocity Centelines
d1n
d1f
d1m, d2m
d1f
V
y/D
2.5
2
1.5
1
0.5
0
0
2
4
6
8
10
12
14
16